JOURNAL OF GEOPHYSICAL RESEARCH, VOL. 106, NO. C11, PAGES 26,943–26,957, NOVEMBER 15, 2001

Inertial oscillations in the Korea Strait

G. A. Jacobs, J. W. Book, H. T. Perkins, and W. J. Teague

Naval Research Laboratory, Stennis Space Center, Mississippi USA

Abstract. Inertial oscillations (IO) are examined in the Korea Strait based on measurements from 13 acoustic Doppler current profilers covering the time period May 1999 through March 2000. Strong IO responses to wind stress occur during summer. A simple linear model predicts that winter wind stress is expected to generate inertial responses of the same order of magnitude as those in summer. However, the observed winter IO response is much weaker than predicted. During summer, the currents within the mixed layer and below the mixed layer are of comparable amplitude but in opposite directions. The depth at which the currents reverse directions varies throughout the year as the mixed layer deepens from about 40 m during summer to the bottom of the water column in November. During winter, the velocity structure is more uniform in depth with currents in the same direction throughout the water column. One possible explanation for these phenomena is related to the combined effect of the strait boundaries and the strong summer stratification. The stratification prevents the wind stress momentum flux from mixing downward below the thermocline and thus allows the development of a bottom current separate from the surface current. Such a velocity structure is necessary to satisfy the no-flow condition through the land boundaries.

1. Introduction

The Korea Strait is the connection between the Yellow and East China Seas and the Sea of Japan. The transport through the strait varies from 1 Sv to 5 Sv with changes occurring over time periods of less than 10 days [*Jacobs et al.*, 2001]. The water mass characteristics within the Yellow and East China Seas [*Hur et al.*, 1999] strongly affect conditions within the Sea of Japan. Understanding the dynamics underlying and controlling variations within the strait is critical to understanding the connections between these marginal seas.

Inertial oscillations (IO) are a fundamental solution to the unforced simplified ocean dynamics. Thus forcing perturbations and the availability of energy in the ocean system are expected to generate IOs. One unique example is the available energy within horizontal temperature gradients interacting with vertical mixing that may generate sustained IOs [*Pedlosky and Stommel*, 1993]. Wind forcing is one of the principal observed initiators of IOs [*Pollard*, 1970; *Pollard and Millard*, 1970; *Weller*, 1982]. In particular, IOs have been examined after the passage of hurricanes or typhoons [*Brink*, 1989; *Shay and Chang*, 1997; *Firing et al.*, 1997].

Inertial oscillations are mainly a balance between the time rate of change of velocity and the Coriolis force [*Gill*, 1982]. The theoretical oscillation frequency f (the Coriolis parameter) varies from 1.102 cycles per day (cpd) at the southern limit of our mooring array (33.35°N) to 1.160 cpd at the northern limit (35.35°N) with an average value of 1.132 cpd at the mean latitude. Several factors alter the predicted frequency including latitudinal variations in the Coriolis parameter [*Ripa*, 1997], divergence in the quasi-geostrophic flow field [*Weller*, 1982], vorticity in the quasi-geostrophic flow field [*Mooers*, 1975; *Perkins*, 1976], and dissipation of energy through friction or other means [*Pollard*, 1970]. The latitudinal variations in the Coriolis parameter discussed by *Ripa* [1997] are also capable of generating mean eastward or westward drift.

One difficulty in observing IOs has been obtaining data with sufficient temporal and spatial extent to examine the three-dimensional nature of the oscillations [*Firing et al.*, 1997]. The development of trawl-resistant bottom mounts has allowed long-term moorings to be deployed and high-accuracy current data to be returned from areas on the continental shelf. Fishing activities have long hampered efforts to obtain these types of data [*Kawatate et al.*, 1988]. In this paper, we examine data from 13 moorings deployed in the strait from May 1999 through March 2000. Twelve acoustic Doppler current profilers (ADCP) are deployed along two lines in the Korea Strait, and one ADCP is deployed in the western channel between the Korea peninsula and Tsushima Island (Figure 1). The southern line (southwest of Tsushima Island) covers the inflow to the strait, and the northern line (northeast of Tsushima Island) covers the outflow from the strait.

The strait regional geometry is quite different from the open ocean character of many previous IO observations. The semienclosed character appears to influence the dynamics, as IO correlations are larger in the across-strait direction than in the along-strait direction. The vertical IO structure in deep open ocean areas is a strong response to wind forcing in the surface mixed layer with a weaker response below the mixed layer [*Brink*, 1989; *Firing et al.*, 1997]. Results here indicate an IO velocity reversal below the depth of the mixed layer similar to previous observations and analytic studies near coastlines [*Millot and Crepon*, 1981; *Schahinger*, 1988; *Federjuk and* Allen, 1996]. Currents within the mixed layer are directed oppositely to currents below the mixed layer with amplitudes below the mixed layer comparable to those within the mixed layer.

Paper number 2000JC000509.

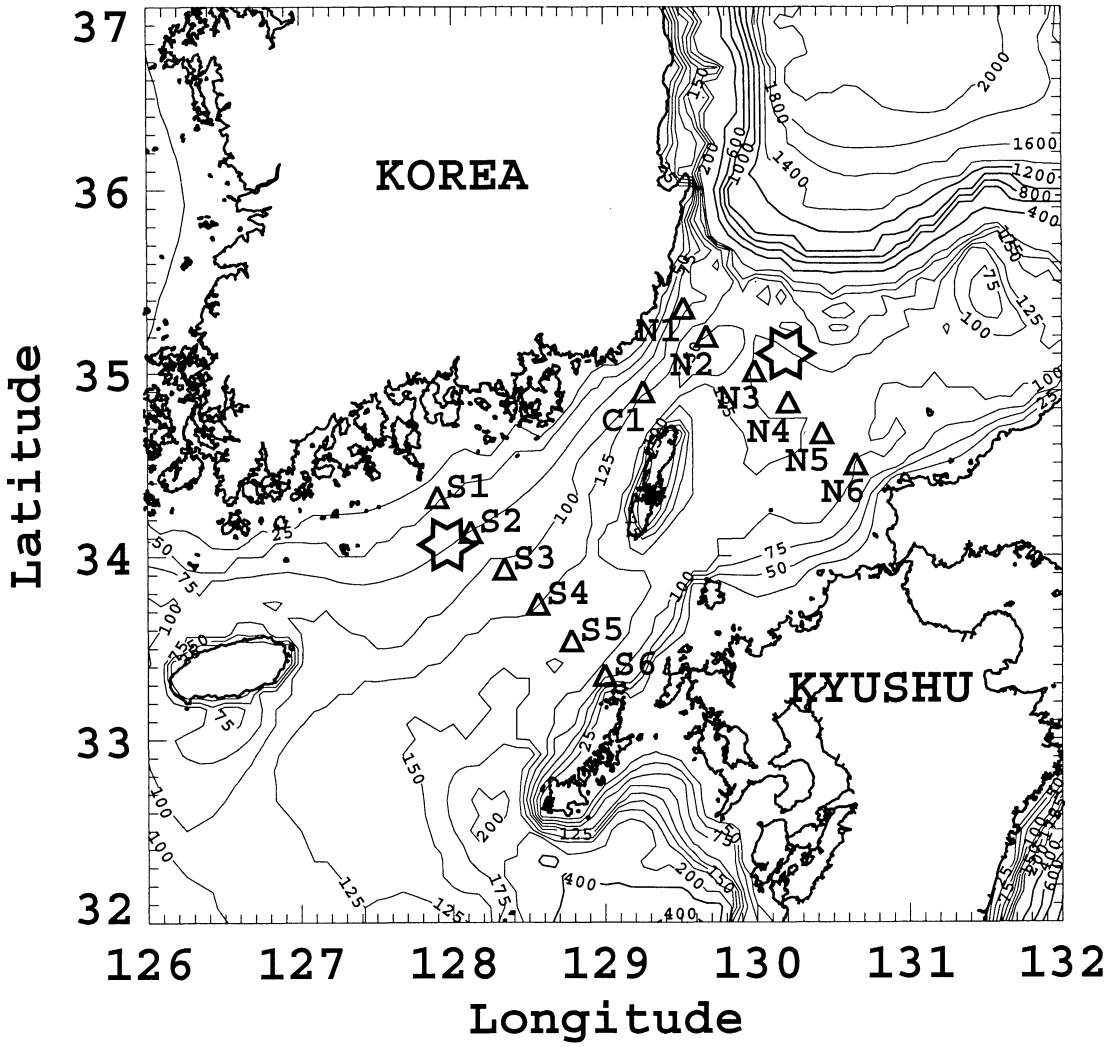

Figure 1. Acoustic Doppler current profiler (ADCP) moorings deployed along two lines, northeast (N1 through N6) and southwest (S1 through S6) of Tsushima Island and in the narrow between the Korea peninsula and Tsushima Island (C1), from May 1999 through March 2000. The two stars are points at which the wind stress and its response are examined (Figure 5 and Figure 6).

The vertical stratification within the strait changes dramatically from winter to summer. The majority of the transport through the strait originates from the continental shelf in the Yellow and East China Seas. The regional heat flux generates a strong summer thermocline near 40 m [*Hu*, 1994]. During winter, the heat flux and stronger wind stress combine to generate a uniformly mixed water column. The IO activity during winter is significantly reduced in relation to summer even though winter wind stress is expected to generate IOs as large as those during summer.

The mooring array and instrumentation are described (section 2), and the vertical and horizontal IO structures are then examined (section 3). We discuss possible causes for the IO structure (section 4). Our conclusions then follow (section 5).

2. Instrumentation

ADCP moorings were deployed along two lines in the strait during May 1999 (Figure 1). Six bottom-mounted trawl-resistant moorings were placed along the line northeast of Tsushima Island (N1 through N6), and six were placed along the line southwest of Tsushima Island (S1 through S6). In October 1999, a maintenance cruise was conducted during which the instruments were recovered, refurbished, and redeployed. An additional instrument was deployed between the Korean peninsula and Tsushima Island during the second cruise (C1). The instrument recovery cruise took place in March 2000. The ADCPs measure velocity profiles with a 4-m vertical bin interval (except at N2 and S5, which measured with a 2-m vertical bin interval). Each instrument provides velocity samples at 15-min intervals. Data near the surface are contaminated by interference of the ADCP acoustic beam with the water surface. The distance from the surface at which the interference occurs varies with instrument deployment depth. The ADCPs in the deep channels (140 m) measure currents to within about 20 m of the surface, while ADCPs in the shallower regions (100 m) measure currents to within about 10 m of the surface. The closest measurements to the surface occur at mooring S2 (55-m depth), which measures to within 5 m of the surface.

Tidal variability within the strait is strong. This study is

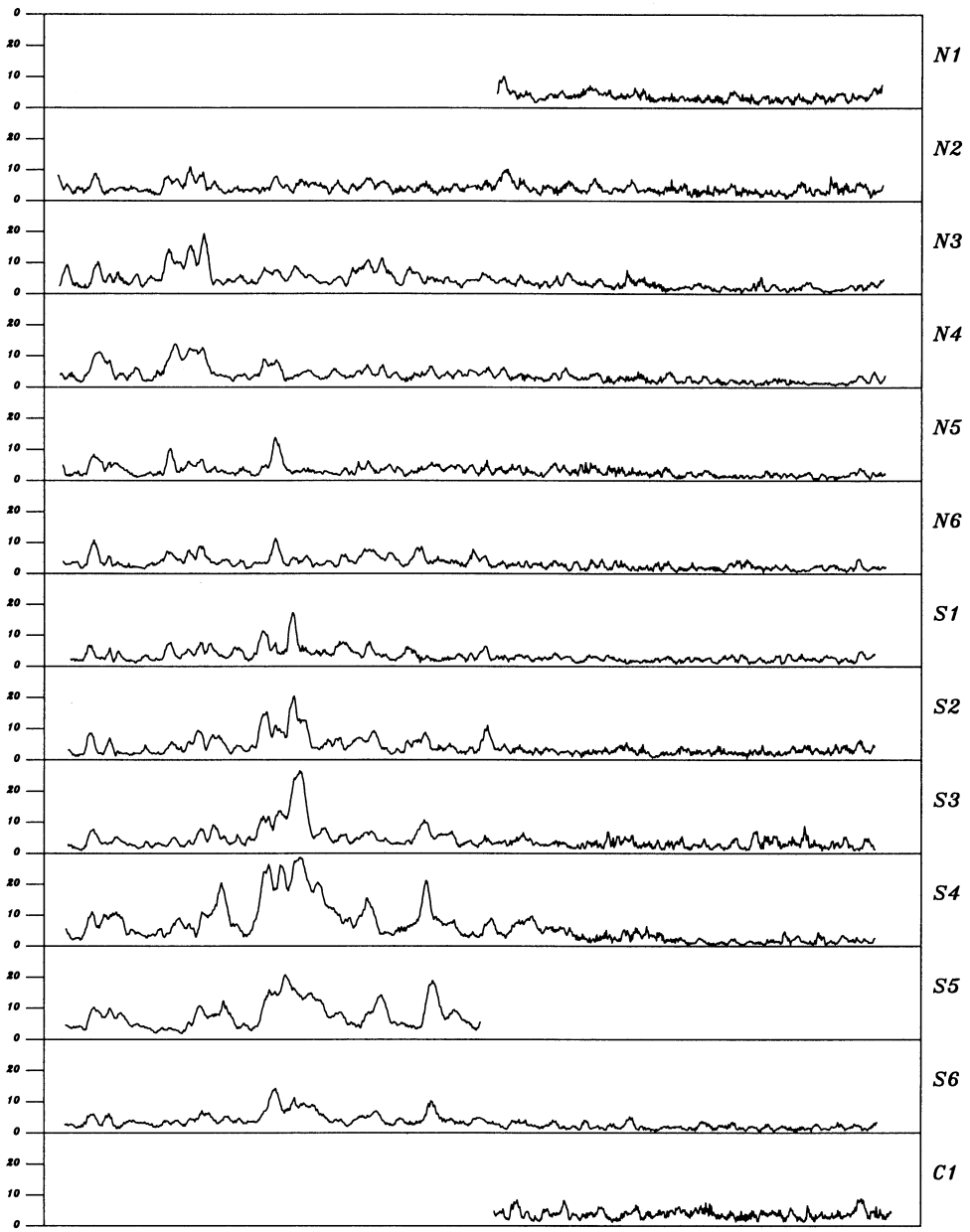

Figure 2. Vertically averaged amplitude of the negative rotary spectra at only 1.10 cpd for the 13 ADCP moorings indicating the main peaks that occur in May through September. Very little variability occurs during winter. The variability in the southern line during July and August is correlated to the passage of a typhoon event traveling northeast and passing across Kyushu (see wind stress in Figure 5).

concerned with nontidal variations. To remove the tidal variability, the eight main tidal constituents (M2, S2, K1, O1, N2, P1, K2, and MU2) are removed by harmonic analysis from the time series of u (eastward) and v (northward) velocities. This process is conducted for each velocity component at each depth bin independently. *Teague et al.* [2001] examine the tidal constituents in detail including the fraction of the total variability at tidal frequencies as well as the vertical structure of the tidal constituents. Tides account for 20% to 60% of the velocity variability depending on depth and mooring location. There are of course additional active tidal constituents, though the residual tidal variability is much smaller than the nontidal velocity variability. This is apparent in the spectra examined in section 3.

3. Inertial Oscillation Structure

3.1. Rotary Spectra

We first examine the temporal changes in energy distributed near the inertial frequency. An analysis technique similar to that of *Brink* [1989] is performed on each ADCP data set independently, and each depth level is treated independently. An amplitude spectrum is computed at each point in time using data contained in a window centered at each time. The window width is discussed shortly. The amplitude spectrum is computed by a least squares fit. The amplitude of each frequency is computed separately to avoid interference between frequencies that may be closer than the Fourier frequency of the window width. The ability to choose a

relatively fine frequency discretization allows spectral peaks to be better located. This procedure does not change the spectral peak leakage characteristics, which are determined by the window width. The least squares fitting procedure allows data dropouts to be easily handled without interpolation or filling in of data. The least squares fit for each frequency computes the function coefficients of a constant and linear trend and a cosine and sine wave of the specified frequency. The constant and linear trend prevents variability at time periods longer than the window width from biasing the spectral estimates.

We initially use a 3-day window width. A shorter window width allows temporally local oscillations to be better localized in time at the expense of wider leakage in frequency. A wider window width allows better frequency location at the expense of wider leakage in time. The rotary spectra amplitude is computed over the frequency range from 0.5 cpd to 2.5 cpd. The inertial frequency at the mooring array central latitude (34.35°N) is 1.132 cpd. To compress the presentation of results, the amplitude spectra are averaged over depth resulting in one time series of inertial oscillation amplitude for each mooring. An important point is that we average the amplitude spectra over depth rather than averaging velocity over depth and then computing the spectra. A more detailed examination of the vertical structure is presented in section 3.2.

The vertically averaged negative rotary spectra (Plate 1) contain many peaks localized in time and in frequency. The peaks correspond to a time interval during which variability is dominated by oscillations at a particular frequency. A majority of the peaks occur during summer, and there is a large decrease in the occurrence of peaks after November. Most of the peaks are centered on a frequency of 1.10 cpd at most of the mooring locations. The amplitude of the negative rotary spectra at just 1.10 cpd (Figure 2) more clearly indicates the times at which energy maxima occur. Peaks occur simultaneously at several moorings indicating features with large spatial scale that may be generated by forcing that has large spatial scale. The amplitude peaks that appear in the northern and southern lines are more correlated among observations by instruments in the same line. For example, the June peaks in N2 through N6 do not appear strongly in the southern line instruments. Similarly, the peaks during July and August within the southern line do not appear strongly in the northern line.

There are no large continuous bands of energy or periodically repeating peaks near 1 cpd or 2 cpd. Small-amplitude energy bands are apparent in some of the spectra such as in S6 at 2 cpd (Plate 1). Such features are indications of residual tide energy. Thus after the eight tidal constituents are removed by the least squares analysis (section 2), the residual tidal variability is much less than nontidal variability.

The 3-day window provides a Fourier frequency of 1/3 cpd. Thus energy at an isolated frequency appears in the analysis to be smeared over a range of frequency space from the peak's frequency to 1/3 cpd to either side. This produces peaks that appear to cover a large frequency band in Plate 1. If the temporal window is broadened, the frequency leakage is diminished. To examine the primary frequency contained in the observed oscillations, we compute the above analysis using a 20-day window. This provides for spectral leakage width of 0.05 cpd. The spectra are computed over the frequency range from 0.9 to 1.4 cpd (Plate 2). The spectral peaks are clustered near 1.10 cpd at most of the mooring locations. This is the value of the inertial frequency at the southernmost mooring (1.102 cpd at 33.35°N). Thus the dominant oscillation frequency is slightly lower than the inertial frequency.

The lower than theoretical frequency has been observed previously. *Kundu* [1976] and *Millot and Crepon* [1981] observe spectral peaks at frequencies both lower and higher than the expected inertial frequency. Frequencies higher than the inertial frequency are associated with internal waves. The inertial frequency is a theoretical lower bound of the internal wave frequency. The lowering of the inertial frequency is possible through the larger-scale flow altering background vorticity [*Mooers,* 1975; *Perkins*, 1976; *Weller*, 1982]. The mean flow through the strait is higher within the strait center and lower near the strait boundaries. Thus a background shear or vorticity exists within the mean flow that would alter the inertial frequency. The effect would have opposite signs on the north and south sides of the center of the strait. If this were a large factor, then the inertial frequency would be higher than the Coriolis parameter on one side of the strait (the north side) and lower on the other side. This is not observed in the rotary spectra. The peak energy is consistently concentrated at frequencies lower than the inertial at moorings both north and south of the strait center. One additional possibility for lowering the inertial frequency is the dissipation of IO energy by bottom friction or turbulent mixing downward from the surface layer [*Pollard,* 1970].

3.2. Spatial Structure

First we examine the vertical structure at each mooring site and then the correlations between moorings. The analysis is limited to the frequencies at which a majority of the amplitude peaks occur (Plate 2). The analysis frequency is taken to be 1.10 cpd, which is just below the inertial frequency. The 1.10 cpd sine and cosine coefficients for the eastward and northward velocity at each time and depth define the velocity vector field. Even though we construct a velocity field using the sine and cosine coefficients, the velocity field is not periodic as the sine and cosine coefficients change with time. Plate 3 shows the velocity direction at each depth relative to the surface velocity. The angle required to rotate the surface velocity to northward is used to rotate the velocity vector at each depth. For this particular analysis we use the spectra defined by using the 20-day window. The reason for this is to reduce noise contained in the spectra using the 3-day window.

During May through September, the lower-depth velocity direction is reversed in relation to the near-surface velocity. The depth at which the direction reverses varies between mooring locations from 20 m to 40 m. From October through November, the velocity reversal depth increases dramatically, and from December onward the deeper waters are directed more toward the direction of the surface velocities. The implication is that a strong baroclinic flow exists through the summer, and the flow gradually changes to barotropic in the winter.

The correlations between moorings at 1.10 cpd are examined through an extended empirical orthogonal function (EEOF) analysis. Since the peaks in the rotary spectra (Plate 1) are more correlated between instruments along each line than between instruments in separate lines, we restrict the EEOF to variations along only one line. In particular, the south line indicates larger variations. First, the spectral coefficients from the 3-day window at 1.10 cpd are used to reconstruct the velocity variability at only that frequency.

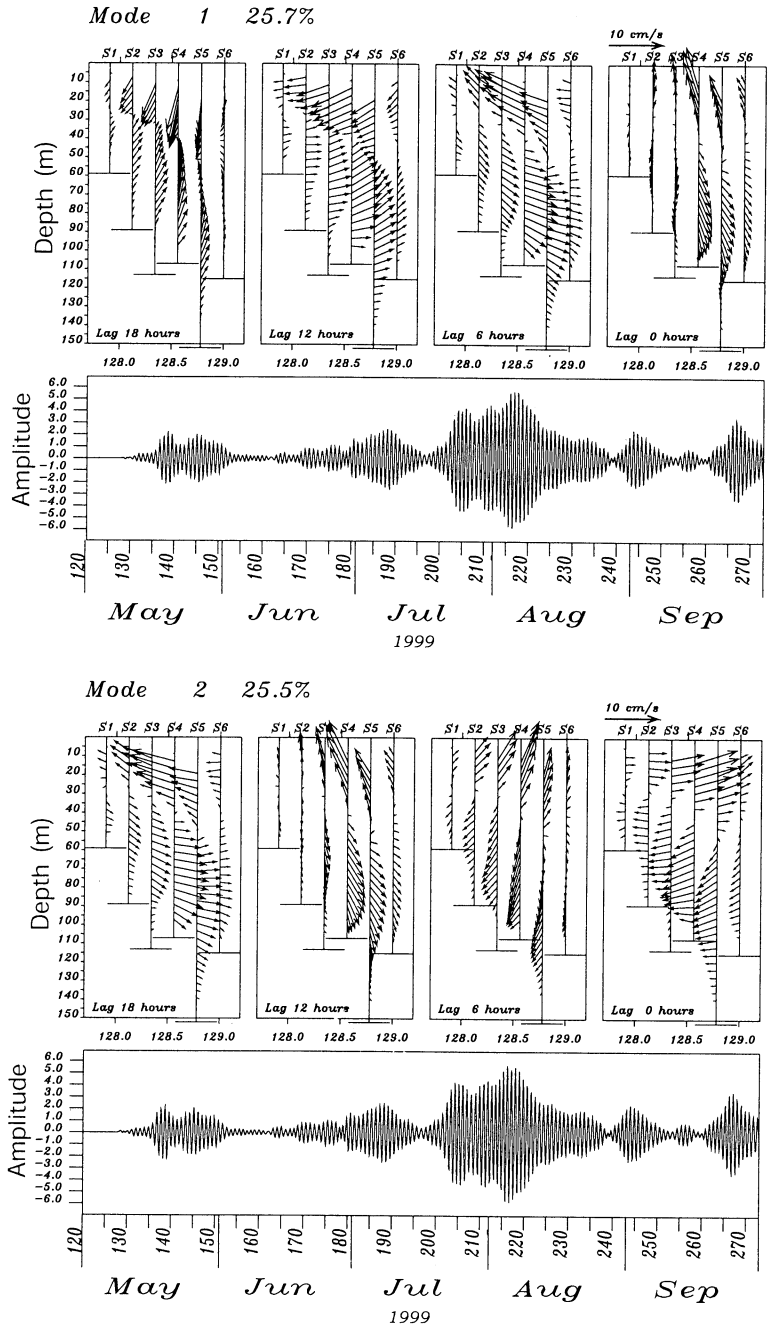

Figure 3. Extended empirical orthogonal function (EEOF) using only summer data with four lagged data sets from 18- to 0-hour lags indicating the temporal development at the southern moorings of the most correlated variability in space (horizontal and vertical) and time. This is based on the variability at only 1.10 cpd; so the clockwise rotation of currents is apparent. The time series indicates when this type of development occurs. The currents at a particular time are obtained by multiplying the amplitude of the time series by the spatial amplitude. Thus peak currents reach 50 cm/s.

Each time series of u or v velocity is treated as an independent time series. In order to construct the EEOF, all the time series are duplicated. The duplicated time series are then lagged (moving events backward in time) by 6 hours. All the original time series are again duplicated and lagged backward by 12 hours. One more data set is created lagged by 18 hours. Now we have four sets of time series, lagged at 0, 6, 12, and 18 hours. The time series contained within all these data sets are brought together into a standard EOF analysis. Normally, an EOF analysis derives structures that are most correlated in space without taking into consideration any time correlation characteristics. By including the time-lagged data sets, we force the EOF analysis to take time correlations into account as well. Each EEOF mode contains the spatial structure at four lagged times, and these four spatial structures indicate how an event is correlated over a short time period. Thus the results provide a synopsis of the rapid temporal development of an event as well as an indication of when in the data record the particular development occurs.

Because there are marked differences in the summer and

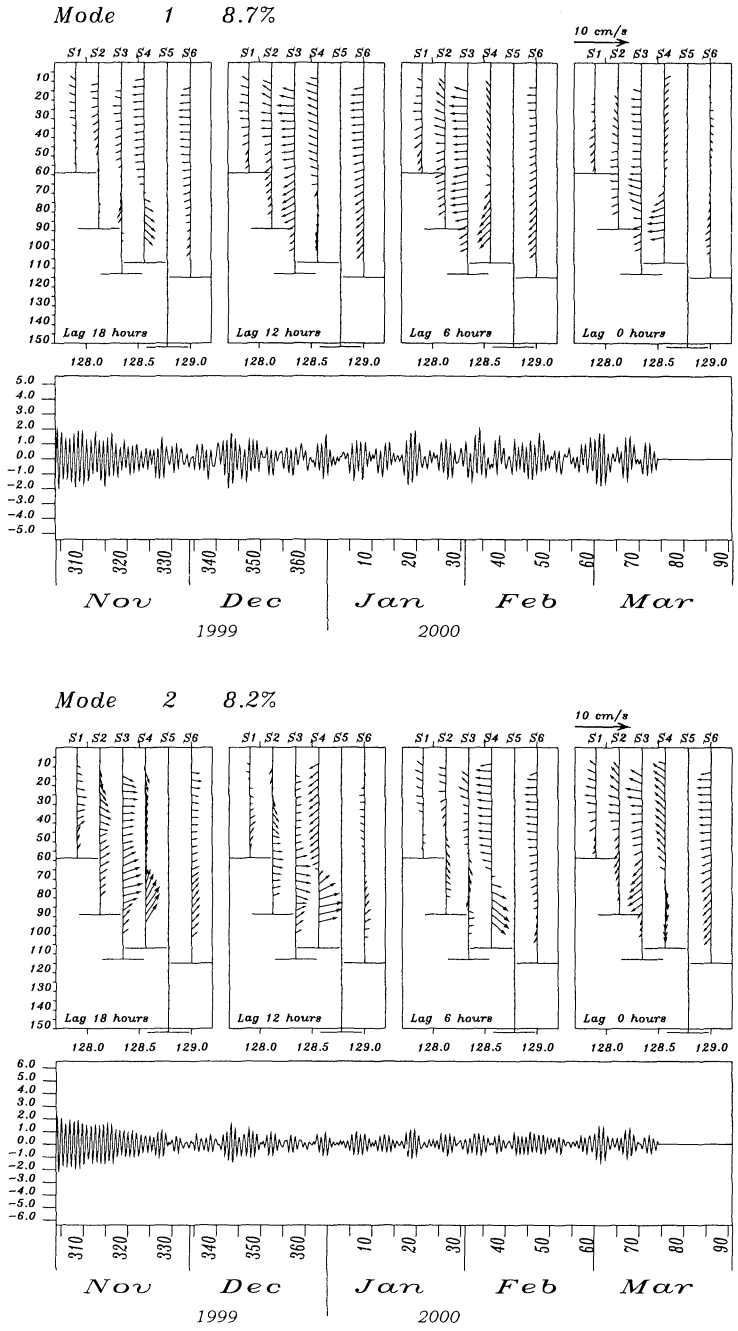

Figure 4. Same as Figure 3, except using data only during winter. The winter extended EOF does not contain the clockwise rotation as the summer data. Thus most of the variability at the 1.10 cpd is not associated with inertial oscillations in winter.

winter spectra, we perform the EEOF analysis separately over these two time periods. We use data from May through September for summer and November through March for winter. The first two summer EEOF modes (Figure 3) contain 25.7% and 25.5% of the total variability. The currents within the four lagged data sets indicate the development of an event through 18 hours, and the time series indicates when this particular type of development takes place. The third and fourth summer EEOF modes each explain only 4.6% of the variability. Thus the summer IO is dominated by the first two modes, which combine to form the equivalent of a cosine and sine function to replicate the variations at 1.10 cpd. The characteristics of the two modes are similar; so the discussion is applicable to both modes.

At each mooring depth, the development through the lagged data sets indicates the clockwise velocity vector rotation. The oppositely directed surface and bottom currents are also apparent. With only the first two modes, the temporal variations of the velocity reversal depth are not apparent. The higher modes contain this information. The time series is normalized to have an RMS variability of 1, and the spatial structure contains the variability. At any particular time, the actual velocity magnitude implied by this mode is equal to the spatial structure multiplied by the time series amplitude. The

peak time series amplitude reaches a value of about 5, and the peak implied currents are about 50 cm/s at the surface and slightly less at depth.

The winter EEOF analysis (Figure 4) indicates the much smaller amplitude variability relative to summer. The fraction of variability explained by the first two modes is 8.7% and 8.2%, indicating that there is no single dominant process throughout the winter record. Also, the development of the velocity field through the lagged fields does not indicate the clockwise rotation that would be expected from inertial oscillations. Thus it appears that the small amount of energy near the inertial frequency during winter is not associated with inertial oscillations or a separate process of amplitude larger than the inertial oscillations is masking any inertial oscillation response. The variability at the 1.10 cpd frequency in winter is likely a component of some other process such as the response to the typical northerly wind bursts.

4. Discussion

The IO character observed here is similar in many respects to that observed in previous studies. The main energy is located in the mixed layer and, as will be shown shortly, is strongly associated with wind stress events. Many studies previously have demonstrated the close connection between wind stress and the IO energy [*Pollard and Millard*, 1970; *Kundu*, 1976]. Also, the near-surface and near-bottom IO currents are oppositely directed. The oppositely directed currents have been observed [*Millot and Crepon*, 1981; *Keen and Allen*, 2000] as well as modeled [*Millot and Crepon*, 1981; *Federjuk and Allen*, 1996].

However, the winter rotary spectra are surprisingly devoid of energy near the inertial frequency (Plate 1). There are numerous possibilities that may generate this observation. First, the winter wind stress may not be conducive to generating IOs. As discussed by *Crawford and Large* [1996], the simultaneous wind stress temporal variation and ocean currents are important to determine the energy transferred from the atmosphere to the ocean. Second, the ocean system itself changes from summer to winter so that the response to similar wind forcing may be quite different.

To determine if the winter wind stress is conducive to generating IO energy in the ocean, we implement a simple model. This model is similar to that used by *Pollard* [1970] and *Pollard and Millard* [1970] and later slightly modified by *D'Asaro* [1985]. The model treats the mixed layer as a uniformly mixed layer of constant density in which momentum is instantaneously mixed to the base of the layer. Thus the equations used are the linear barotropic equations for a layer of constant density and no surface height variation:

$$\frac{\partial u}{\partial t} = fv - ru + \frac{\tau_x}{\rho H}$$
$$\frac{\partial v}{\partial t} = -fu - rv + \frac{\tau_y}{\rho H}, \tag{1}$$

where r is a dissipation constant, f is the Coriolis parameter, ρ is the mixed layer density, H is the mixed layer depth, and (τ_x, τ_y) is the wind stress vector. The steady state solution is the Ekman transport:

$$u_o = \frac{1}{k^2}\left(r\tau_x + f\tau_y\right)$$
$$v_o = \frac{1}{k^2}\left(r\tau_y - f\tau_x\right), \tag{2}$$

where $k^2 = \rho H\left(f^2 + r^2\right)$. The equations governing the deviations from the Ekman transport (the inertial velocities) are then

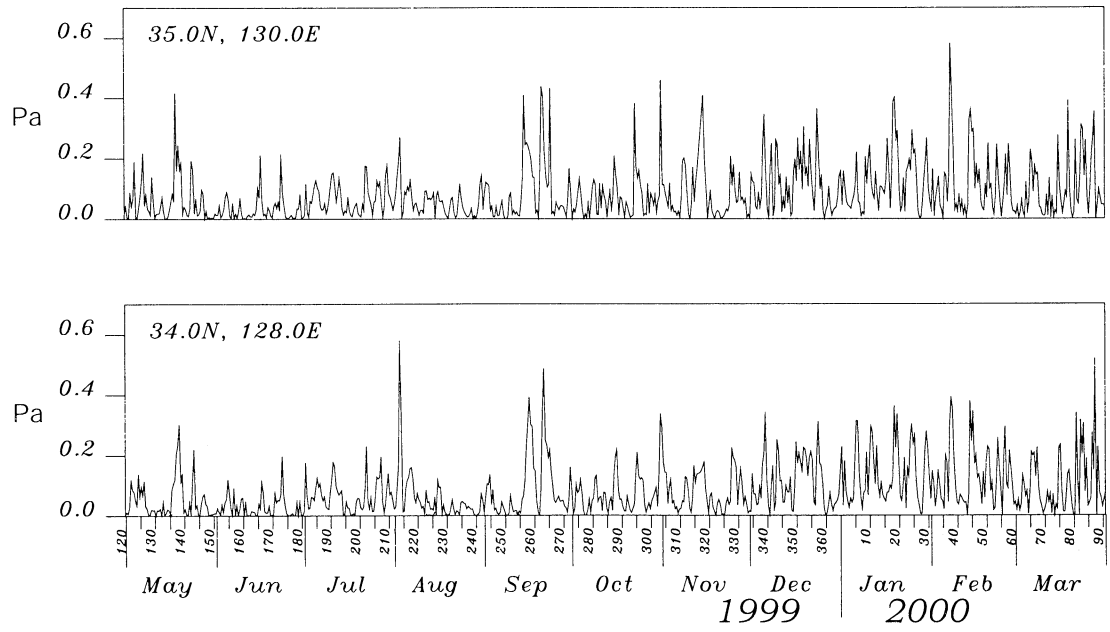

Figure 5. Wind stress magnitude at two points in the Korea Strait (see Figure 1 for positions) indicating events during May and July/August that correlate with the inertial oscillation amplitude. However, increased events of the same amplitude during winter do not appear to generate inertial oscillations (Figure 6).

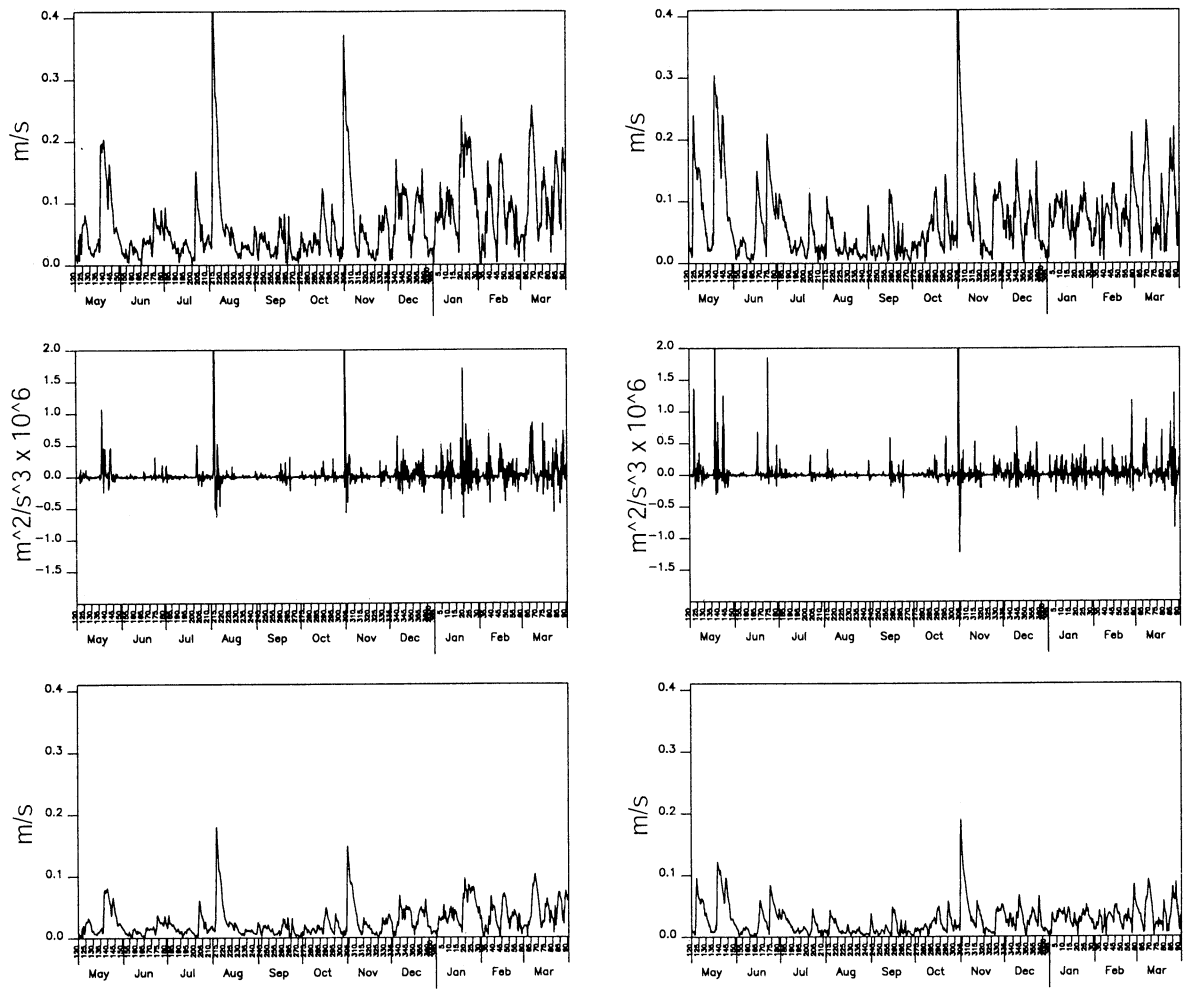

Figure 6. Barotropic mixed layer model providing estimates of (top) inertial velocity amplitude using a 30-m mixed layer depth, (center) energy flux from wind stress, and (bottom) inertial velocity amplitude using a 100-m mixed layer depth. The analysis is based on 6-hourly NOGAPS wind stress at (left) 34°N, 128°E and (right) 35°N, 130°E. High inertial velocity amplitudes in the model at the southern point correspond well with observed inertial oscillation energy at moorings along the south line (Figure 2) during May through September. Similarly, inertial velocity amplitudes at the northern point correspond with observed oscillation energy at moorings along the north line. Winter amplitudes and energy flux events are as large as those during summer. To account for the deepening winter thermocline, the inertial velocity amplitude is recomputed by using a mixed layer depth of 100 m (bottom). Winter still indicates inertial oscillation that would be much larger than that observed (Figure 2). The implication is that another process is preventing inertial oscillations during winter.

$$\frac{\partial u_I}{\partial t} = fv_I - ru_I + \frac{\partial}{\partial t}\left(-\frac{r}{k^2}\tau_x - \frac{f}{k^2}\tau_y\right)$$
$$\frac{\partial v_I}{\partial t} = -fu_I - rv_I + \frac{\partial}{\partial t}\left(-\frac{r}{k^2}\tau_y + \frac{f}{k^2}\tau_x\right). \quad (3)$$

From the momentum equations (3), the equation governing the specific kinetic energy rate of change is

$$\frac{\partial}{\partial t}\left(\frac{1}{2}\left(u_I^2 + v_I^2\right)\right) = -r\left(u_I^2 + v_I^2\right) + u_I\frac{\partial}{\partial t}\left(-\frac{r}{k^2}\tau_x - \frac{f}{k^2}\tau_y\right) + v_I\frac{\partial}{\partial t}\left(-\frac{r}{k^2}\tau_y + \frac{f}{k^2}\tau_x\right). \quad (4)$$

The energy rate of change is forced by dissipation in the first term plus a flux from surface wind stress. Note that the surface wind flux energy depends on the inner product of the inertial velocity with the wind stress time rate of change. In a system with no dissipation ($r = 0$), a wind stress time rate of change 90° to the right of the instantaneous inertial velocity would provide the most efficient transfer of energy to the ocean. This is the condition that determines if a particular wind stress event is conducive to adding energy to the inertial velocity.

We use this system of equations to test the wind stress ability to force IOs. The wind stress is from the Navy Operational Global Atmospheric Prediction System (NOGAPS) [*Hogan and Brody,* 1993; *Rosmond,* 1992; *Hogan and Rosmond,* 1991; *Toll and Clune,* 1985]. Two points surrounding the Korea Strait are chosen (Figure 1). The wind

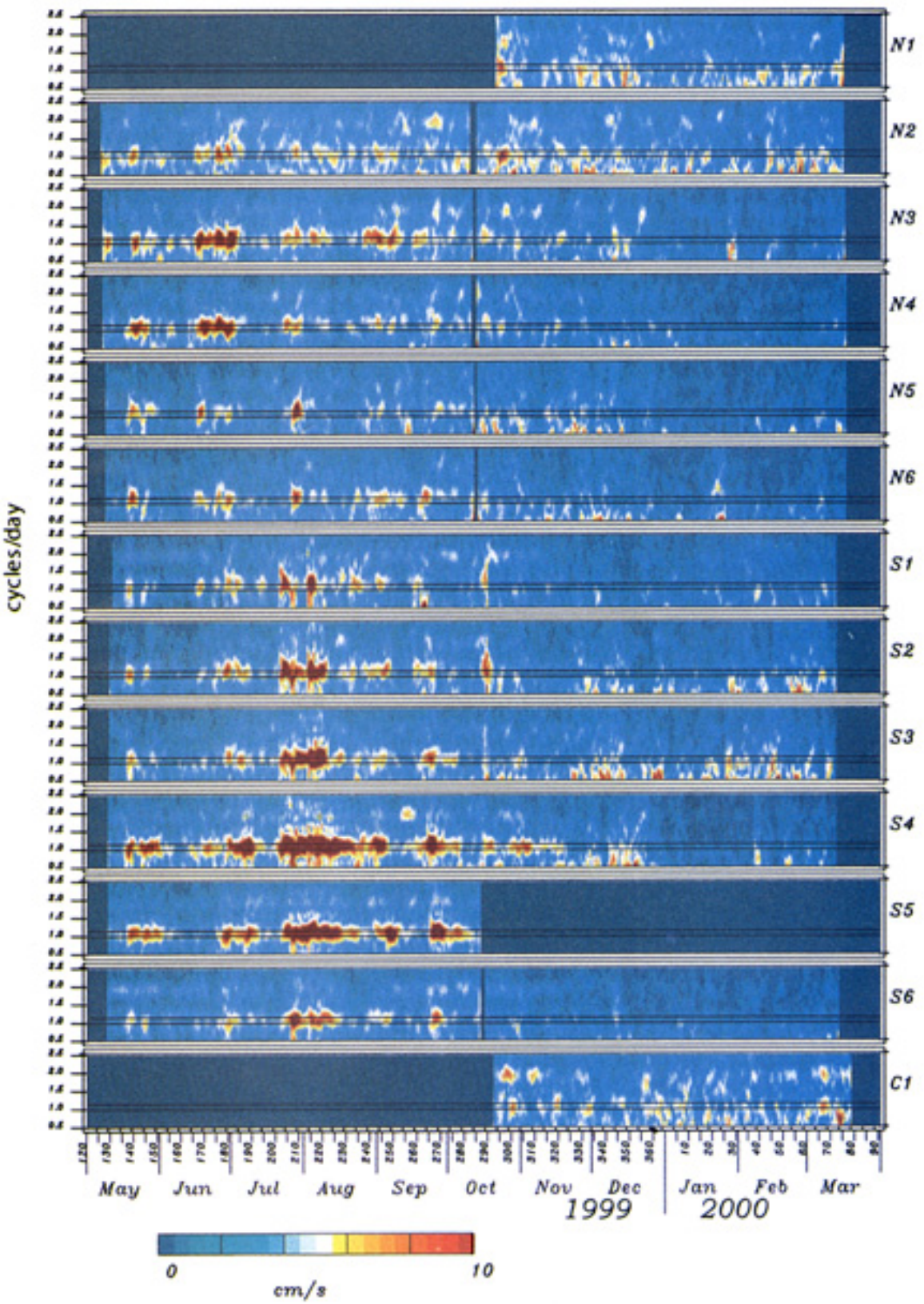

Plate 1. Negative rotary spectra computed by using 3 days of data centered at each point in time. The spectra at all depths are averaged together for each mooring. The 3-day window provides a good indication of when inertial oscillation events occur. A longer 20-day window provides an indication of the frequency of the events (Plate 2). The two horizontal lines in each plot are at the 1 cpd and 1.15 cpd frequencies.

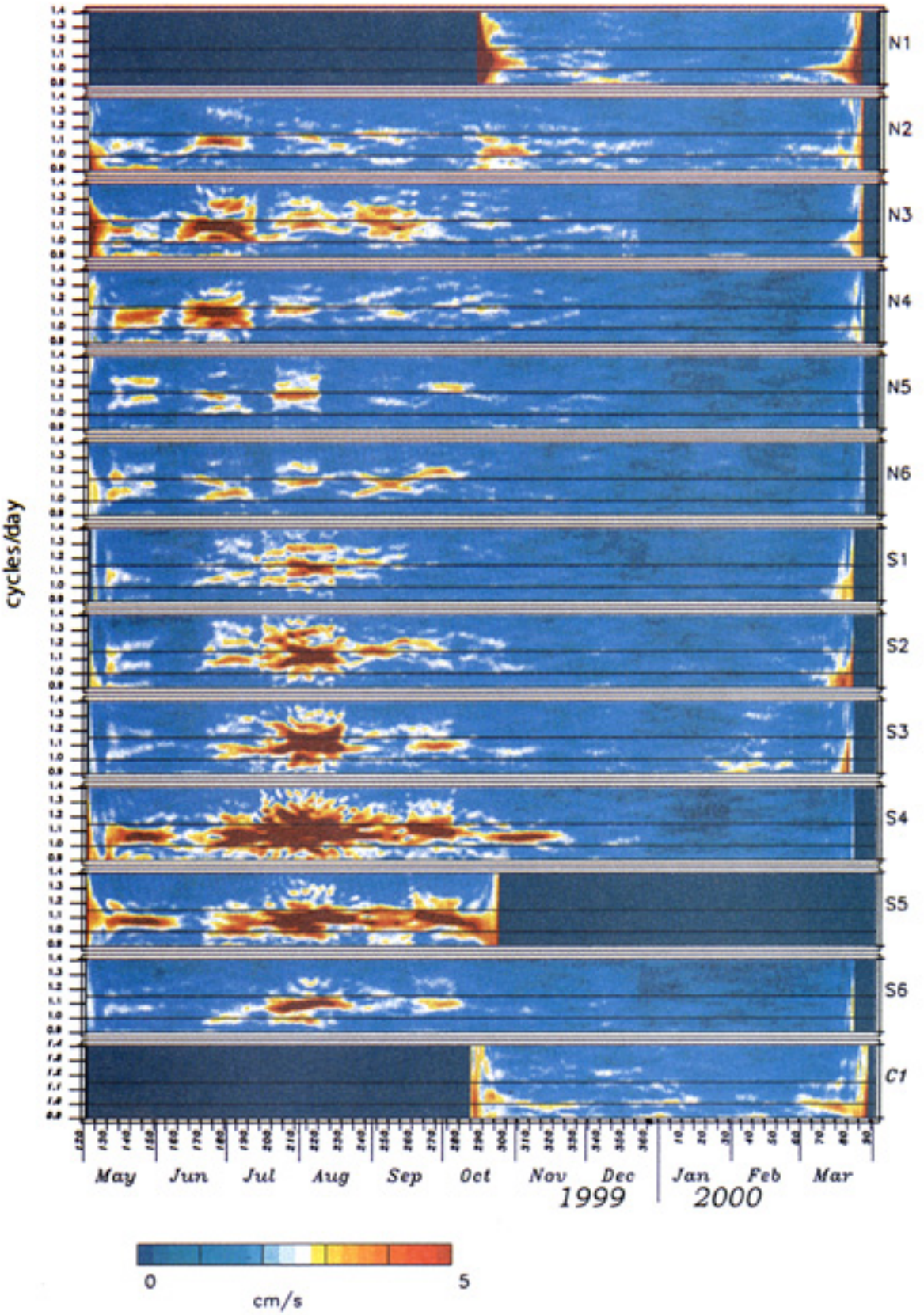

Plate 2. Time-varying amplitude spectra using a 20-day window indicates the frequency at which the energy is occurring. The 20-day window provides a frequency resolution of 0.05 cpd. The two horizontal lines in each plot are at the 1 cpd and 1.15 cpd frequencies. Most of the energy is at a frequency slightly less than the local inertial frequency.

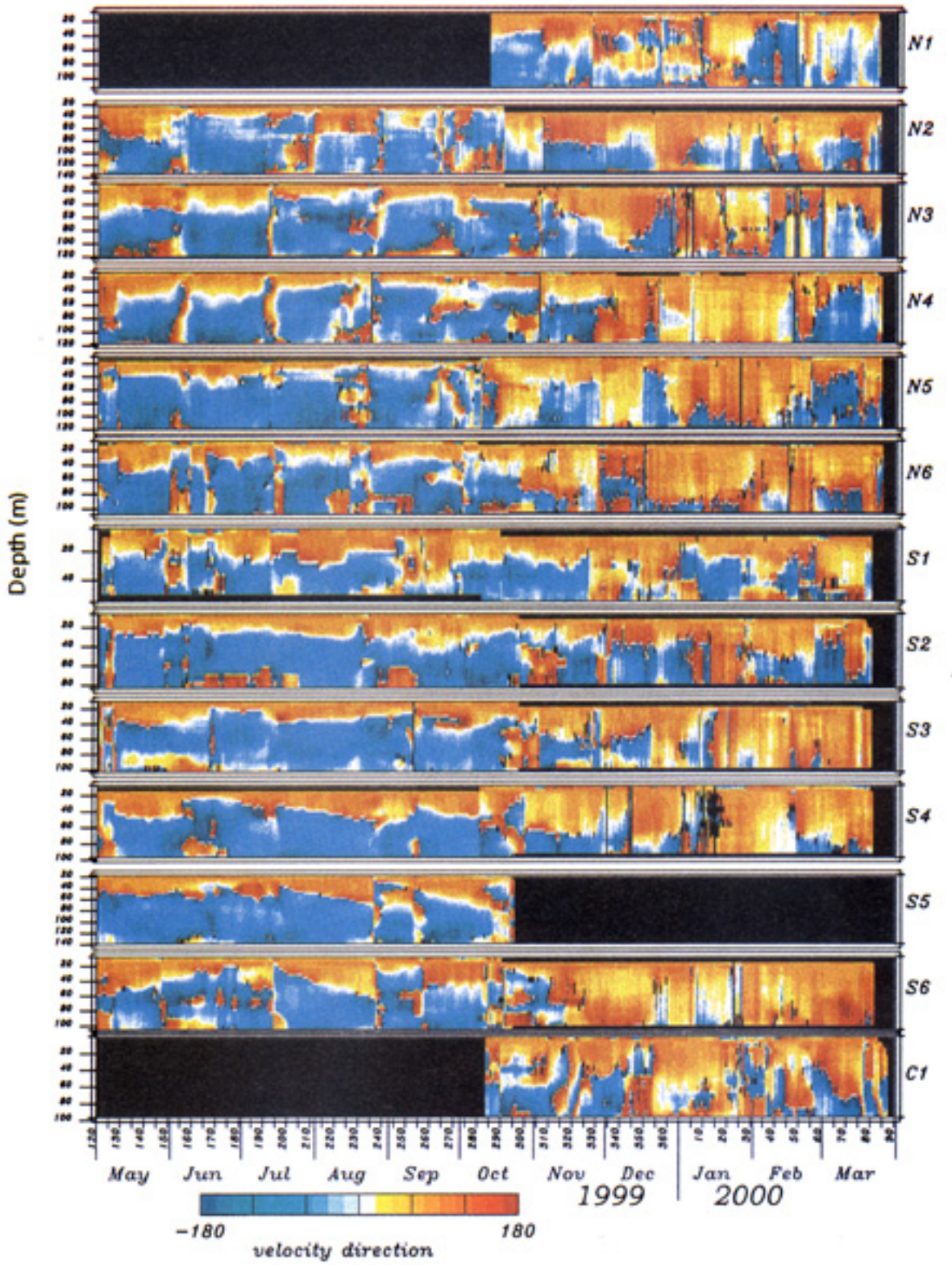

Plate 3. Negative rotary spectra using a 20-day window (Plate 2) used to examine the relative phase throughout the water column. The surface currents at each time are rotated to 90° (northward), and all other currents are rotated by the same amount. In summer, particularly along the southern moorings, the current direction within the mixed layer (about 90°) is in the opposite direction of the currents below the mixed layer (about -90°). During October through November, the level at which currents change directions deepens. The direction reversal is also apparent in the extended EOF analysis (Figure 3 and Figure 4).

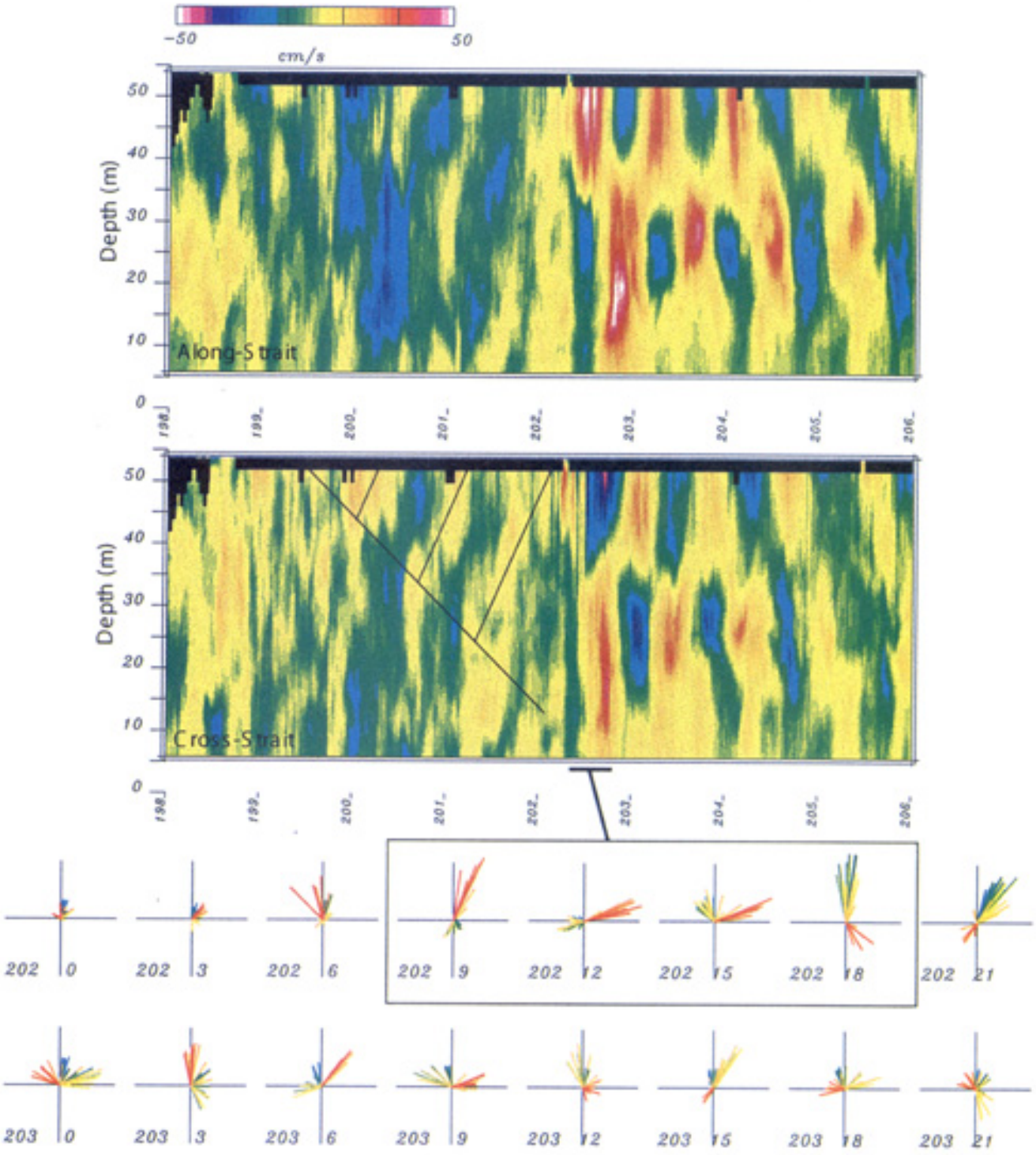

Plate 4. Examples of inertial events at mooring S1 containing an apparently locally generated oscillation beginning on day 199. The phase of the velocity in the cross-strait direction propagates upward, while the group velocity propagates downward. Another larger event begins on day 202. The stick plots in the lower panel indicate the velocity as a function of depth (red near surface, green near the middle, and blue near bottom). The event contains a strong along-strait surface current at day 202, hour 9. As the surface current turns away from the Korea coast on day 202 hour 15, a strong coastward underflow develops by day 202, hour 18. The bottom flow develops over a time period much shorter than that required for the group velocity to propagate to the bottom.

stress magnitude (Figure 5) indicates localized peaks throughout the summer. The spectral peaks near the inertial frequency (Figure 2) are correlated to the wind stress events during summer. However, beginning in October, the wind stress magnitude indicates events of comparable amplitude and in greater abundance than those events during May through September.

As equation (4) indicates, it is not only the wind stress magnitude that is important, but also its time rate of change and the present inertial velocity. The NOGAPS wind stress temporal resolution is 6 hours, and we integrate the wind stress components independently by using a cubic spline interpolation to a 1.5-hour resolution. We integrate the inertial velocity equations (3) forward in time at the same two points at which we examine the wind stress magnitude (Figure 1). The integration method is a fourth-order Runge-Kutta method. We use a mixed layer depth of 30 m and a dissipation time of 4 days (the same as *Pollard* [1970] and *D'Asaro* [1985]). In addition, we calculate the flux term of the inertial energy rate of change equation (4). The NOGAPS wind product time spacing of 6 hours is not sufficient to properly resolve the complete temporal development of all wind events that may generate IO energy. Thus this is one additional error source in our analysis.

The inertial velocity amplitude and inertial energy flux term based on the model (Figure 6) indicate the large events along the south mooring line during summer in agreement with the rotary spectra (Figure 2). The model also indicates events throughout winter of the same magnitude as those during summer. To take into account the winter deepening of the mixed layer to the bottom of the strait, we also run the model with a mixed layer depth of 100 m. Even after taking the deeper mixed layer into account, the model is predicting much larger amplitudes than those observed.

The lack of response to wind events during winter leads us to favor the second possible explanation for the observations. That is, the ocean system itself changes between summer and winter in such a way that it no longer allows an IO response to the wind forcing. The vertical stratification changes dramatically throughout the year (Figure 7). A warm surface layer begins to form in the spring, and the thermocline depth increases during October through November. During winter, the vertical stratification is nearly eliminated. The climatological temperature structure through the year (Figure 7) closely follows the temporal variation in the depth at which the 1.10 cpd current changes direction (Plate 3). A strong thermocline develops near 40 m in summer and erodes in the fall, leaving an unstratified water column through the winter.

The summer stratification inhibits the downward mixing of momentum flux from wind stress. Thus summer wind events force IOs mainly within the mixed layer. The land boundaries along the Korean Strait impose a no-normal flow condition to the continuity equation. If a surface current is directed toward the land (as in the 12-hour or 0-hour lags of EEOF mode 1 in Figure 3), a subsurface current in the opposite direction is one method to balance the transport. This is the typical response predicted at the coastal corner by *Federjuk and Allen* [1996].

In summer, the subsurface current is dynamically separated from the surface current by the strong thermocline that inhibits mixing between the two layers. During winter, the water

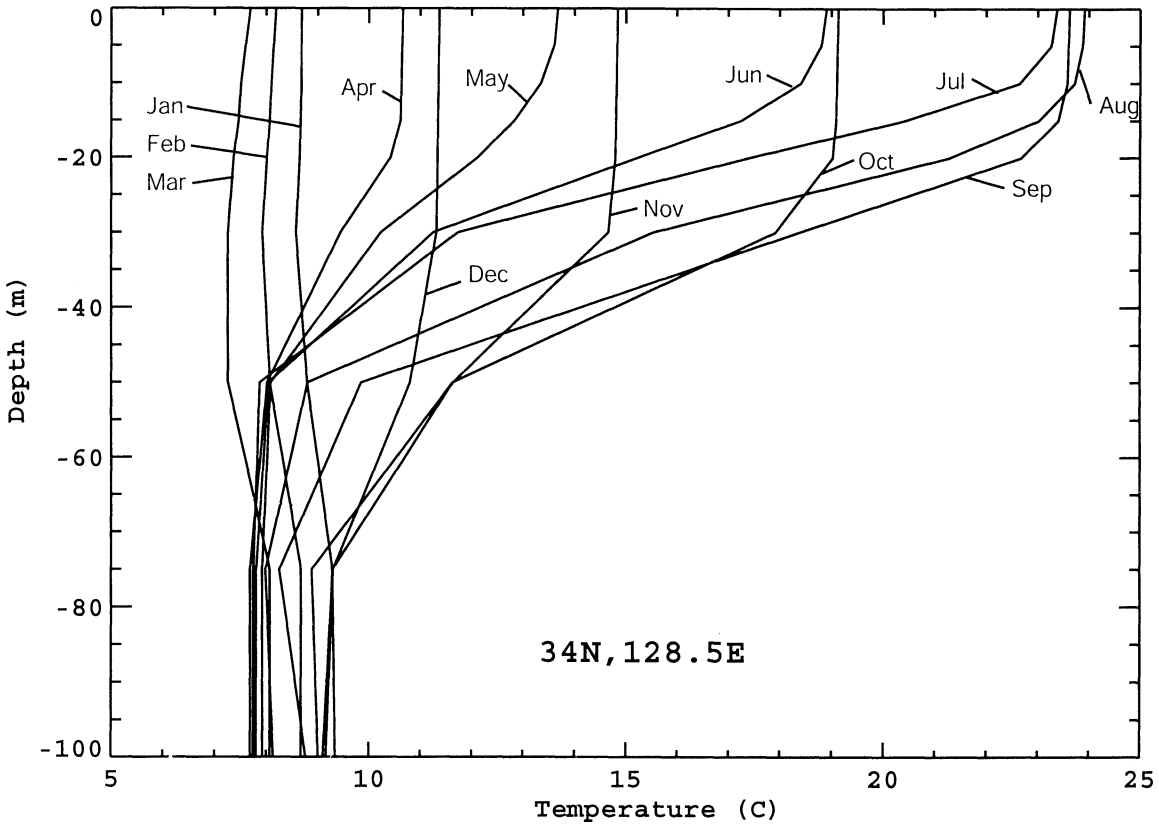

Figure 7. Climatological monthly mean temperature within the Korea Strait indicating the development of the summer thermocline and its subsequent deepening and decay during October through November.

contains no stratification, and wind stress momentum flux is able to easily affect the entire water column. It is more difficult for a current to form below and in the opposite direction to the surface current. Thus the IOs would be suppressed during winter. Instead of generating a surface current and an oppositely directed bottom current during winter, the wind stress would force the water mass toward a coast where the energy would be stored as potential energy of sea level change. The energy would then dissipate through propagating continental shelf waves such as Kelvin waves. The generation and propagation of continental shelf waves in the Yellow and East China Seas due to winter wind stress have been observed and modeled previously [*Hsueh*, 1988; *Jacobs et al.*, 1998]. The spectra (Plate 1) indicate an increased occurrence of low-frequency energy during winter. This energy may be a contribution to the wind stress response at subinertial frequencies.

The difference between the downward propagation of IO energy through wave dynamics [*Kundu*, 1976] and the downward transference of energy by the coastal boundary condition is apparent throughout the ADCP records. One short time sequence of velocity is provided for an example (Plate 4). The examination is made at mooring S1 (closest to Korea along the southern mooring line). The downward propagation of group velocity of inertial oscillations has been observed to be 0.03 cm/s [*Kundu*, 1976]. In Plate 4, the group velocity is similar to this value and requires 2 to 3 days to propagate from the surface to the bottom. However, the event that occurs on day 202 indicates a very rapid downward transfer of energy. The velocity vectors plotted at 3-hour intervals indicate an initially strong surface current parallel to the coast. As the surface current rotates clockwise to a direction away from the coast, a subsurface current rapidly develops in a direction toward the coast. The IO energy within the surface appears to transfer downward much more rapidly than is possible by local group velocity propagation.

We also expect a variation in the thermocline depth associated with the summer IOs. The summer EEOF velocities are larger near the strait center than near the edges. For example, in the 6-hour lag of mode 1 (Figure 3), the surface velocity is directed toward the Korea coast with a small velocity closest to the coast and a large velocity in the strait center. This implies a surface convergence on the Korean half of the strait and divergence on the Japan side. In the subsurface, a divergence occurs in the subsurface on the Korean half of the strait, and a convergence exists on the Japan side. This has implications for the thermocline depth separating the two layers. Suppose we model the strait by a simple two-layer rigid lid system. Let the upper layer transport (velocity times the layer thickness) in the direction from Korea to Japan be modeled as a linear function from the Korea coast

$$\begin{aligned} v &= a\frac{x}{L/2}\cos(ft+\phi) \quad 0<x<L/2 \\ v &= a\frac{L-x}{L/2}\cos(ft+\phi) \quad L/2<x<L, \end{aligned} \tag{5}$$

where x is the distance from the Korea coast and L is the distance across the strait. Assume that the bottom layer transport is opposite to the top layer, and assume that the along-strait variations are negligible. The linearized continuity equation gives time rate of change of the interface depth between the layers as the negative of the divergence of the transport, which is

$$\begin{aligned} v &= -\frac{a}{L/2}\cos(ft+\phi) \quad 0<x<L/2 \\ v &= -\frac{-a}{L/2}\cos(ft+\phi) \quad L/2<x<L, \end{aligned} \tag{6}$$

The interface displacement is given by the integral of (6) over time. Using a width of 100 km for the strait and a transport of 8 m^2/s (a typical value of 0.2 m/s velocity over the upper 40 m), the peak-to-peak thermocline displacement is 4.4 m.

5. Conclusions

Inertial oscillations within the Korea Strait indicate a vertical velocity structure in which the velocity reverses direction near the depth of the mixed layer in summer. While wind stress events occur at the same times as IO events in summer, winter wind events of greater frequency and comparable magnitude occur simultaneously with a marked absence in IO activity. One possible mechanism for explaining the observations is the change in the regional stratification between winter and summer in conjunction with the continuity conditions imposed by the land boundaries. Strong summer stratification prevents wind stress momentum flux from mixing downward and allows for a surface flow toward the boundaries with a subsurface return counter flow. The lack of stratification during winter allows wind stress momentum flux to mix downward and does not allow such a current system to develop.

Acknowledgments. The comments from two anonymous reviewers helped to greatly improve the analysis and quality of this paper. This work was sponsored by the Office of Naval Research (program element PE0601153N) as part of the projects Yellow and East China Seas Response to Winds and Currents, and Dynamical Linkage of the Asian Marginal Seas. This work is contribution JA/7323-00-0020 of the Naval Research Laboratory.

References

Brink, K. H., Observations of the response of thermocline currents to a hurricane, J. Phys. Oceanogr., 19, 1017-1022, 1989.

Crawford, G. B., and W. G. Large, A numerical investigation of resonant inertial response of the ocean to wind forcing, J. Phys. Oceanogr., 26, 873-891, 1996.

D'Asaro, E. A., The energy flux from the wind to near-inertial motions in the surface mixed layer, J. Phys. Oceanogr., 15, 1043-1059, 1985.

Federjuk, J., and J. S. Allen, Model studies of near-inertial waves in flow over the Oregon continental shelf, J. Phys. Oceanogr., 26, 2053-2075, 1996.

Firing, E., R. C. Lien, and P. Muller, Observations of strong inertial oscillations after the passage of tropical cyclone Ofa, J. Geophys. Res., 102, 3317-3322, 1997.

Gill, A. E., Atmosphere-Ocean Dynamics, Academic, San Diego, Calif., 1982.

Hogan, T. F., and L. R. Brody, Sensitivity studies of the Navy global forecast model parameterizations and evaluation of improvements to NOGAPS, Mon. Weather Rev., 121(8), 2373-2395, 1993.

Hogan, T. F., and T. E. Rosmond, The description of the Navy Operational Global Atmospheric Prediction System, Mon. Weather Rev., 119(8), 1786-1815, 1991.

Hsueh, Y., Recent current observations in the eastern Yellow Sea, J. Geophys. Res., 93, 6875-6884, 1988.

Hu, D. X., Some striking features of the circulation in Huanghai Sea and East China Sea, in Oceanology of China Seas, vol. 1, edited

by Z. Di et al., pp. 27-38, Kluwer Acad., Norwell, Mass., 1994.
Hur, H. B., G. A. Jacobs, and W. J. Teague, Monthly water mass analyses in the Yellow and East China Seas, J. Oceanogr., 55, 171-184, 1999.
Jacobs, G. A., R. H. Preller, S. K. Riedlinger, and W. J. Teague, Coastal wave generation in the Bohai Bay and propagation along the Chinese coast, Geophys. Res. Lett., 25, 777-780, 1998.
Jacobs, G. A., H. T. Perkins, W. J. Teague, and P. J. Hogan, Summer transport through the Tsushima/Korea Straits, J. Geophys. Res., 106, 6917-6929, 2001.
Kawatate, K., T. Miita, Y. Ouchi, and S. Mizuno, A report on failures of current meter moorings set east of Tsushima Island from 1983 to 1987, Prog. Oceanogr., 21, 319-327, 1988.
Keen, T. R., and S. E. Allen, The generation of inertial waves on the continental shelf by Hurricane Andrew, J. Geophys. Res., 105, 26,203-26,224, 2000.
Kundu, P. K., An analysis of inertial oscillations observed near Oregon coast, J. Phys. Oceanogr., 6, 879-893, 1976.
Millot, C., and M. Crepon, Inertial oscillations on the continental shelf of the Gulf of Lions-Observations and theory, J. Phys. Oceanogr., 11, 639-657, 1981.
Mooers, C. N. K., Several effects of a baroclinic current on the cross-stream propagation of inertial-internal waves, Geophys. Astrophys. Fluid Dyn., 6, 245-275, 1975.
Pedlosky, J., and H. Stommel, Self-sustained inertial oscillations, J. Phys. Oceanogr., 23, 1800-1808, 1993.
Perkins, H., Observed effect of an eddy on inertial oscillations, Deep Sea Res., 23, 1037-1042, 1976.
Pollard, R. T., On the generation by winds of inertial waves in the ocean, Deep Sea Res., 17, 795-812, 1970.
Pollard, R. T., and R. C. Millard Jr., Comparison between observed and simulated wind-generated inertial oscillations, Deep Sea Res., 17, 813-821, 1970.
Ripa, P., Inertial oscillations and the β-plane approximations(s), J. Phys. Oceanogr., 27, 633-647, 1997.
Rosmond, T. E., The design and testing of the Navy Operational Global Atmospheric Prediction System, Weather Forecasting, 7(2), 262-272, 1992.
Schahinger, R. B., Near-inertial motion on the South Australian shelf, J. Phys. Oceanogr., 18, 492-504, 1988.
Shay, L. K., and S. W. Chang, Free surface effects on the near-inertial ocean current response to a hurricane: A revisit, J. Phys. Oceaogr., 27, 23-39, 1997.
Teague, W. J., H. T. Perkins, G. A. Jacobs, and J. W. Book, Tide observations in the Korea-Tsushima Strait, Cont. Shelf Res., 21, 545-561, 2001.
Toll, R. F., and W. M. Clune, An operational evaluation of the Navy Operational Global Atmospheric Prediction System, Mon. Weather Rev., 113(9), 1433-1440, 1985.
Weller, R. A., The relation of near-inertial motions observed in the mixed layer during the JASIN (1978) Experiment to the local wind stress and to the quasi-geostrophic flow field, *J. Phys. Oceaogr., 12*, 1122-1136, 1982.
Belt, E. S., Post-Acadian rifts and related facies, eastern Canada, in *Studies in Appalachian Geology*, edited by E. Zen et al., pp. 95–113, John Wiley, New York, 1968.
Boatwright, J., Detailed spectral analysis of two small New York State earthquakes, *Bull. Seismol. Soc. Am., 68*, 1117–1131, 1978.
Fetterer, F., D. Gineris, and C. Johnson, Remote sensing aids in sea-ice analysis, *Eos Trans. AGU, 74*, 265, 267–268, 1993.
Orringer, O., Frontal analysis program, *Rep. ASRL TR 1023*, Aeroelastic and Struct. Lab., Mass Inst. of Technol., Cambridge, 1974.

J. W. Book, G. A. Jacobs, H. T. Perkins, and W. J. Teague, Naval Research Laboratory, Code 7323, Stennis Space Center, MS 39529, USA. (book@nrlssc.navy.mil; jacobs@nrlssc.navy.mil; hperkins@nrlssc.navy.mil; teague@nrlssc.navy.mil)

(Received June 26, 2000; revised June 29, 2001;
accepted June 29, 2001.)